

Microanatomy at Cellular Resolution and Spatial Order of Physiological Differentiation in a Bacterial Biofilm

Diego O. Serra, Anja M. Richter, Gisela Klauck, Franziska Mika, Regine Hengge

Institut für Biologie, Mikrobiologie, Freie Universität Berlin, Berlin, Germany

ABSTRACT Bacterial biofilms are highly structured multicellular communities whose formation involves flagella and an extracellular matrix of adhesins, amyloid fibers, and exopolysaccharides. Flagella are produced by still-dividing rod-shaped *Escherichia coli* cells during postexponential growth when nutrients become suboptimal. Upon entry into stationary phase, however, cells stop producing flagella, become ovoid, and generate amyloid curli fibers. These morphological changes, as well as accompanying global changes in gene expression and cellular physiology, depend on the induction of the stationary-phase sigma subunit of RNA polymerase, σ^S (RpoS), the nucleotide second messengers cyclic AMP (cAMP), ppGpp, and cyclic-di-GMP, and a biofilm-controlling transcription factor, CsgD. Using flagella, curli fibers, a CsgD::GFP reporter, and cell morphology as “anatomical” hallmarks in fluorescence and scanning electron microscopy, different physiological zones in macrocolony biofilms of *E. coli* K-12 can be distinguished at cellular resolution. Small ovoid cells encased in a network of curli fibers form the outer biofilm layer. Inner regions are characterized by heterogeneous CsgD::GFP and curli expression. The bottom zone of the macrocolonies features elongated dividing cells and a tight mesh of entangled flagella, the formation of which requires flagellar motor function. Also, the cells in the outer-rim growth zone produce flagella, which wrap around and tether cells together. Adjacent to this growth zone, small chains and patches of shorter curli-surrounded cells appear side by side with flagellated curli-free cells before curli coverage finally becomes confluent, with essentially all cells in the surface layer being encased in “curli baskets.”

IMPORTANCE Heterogeneity or cellular differentiation in biofilms is a commonly accepted concept, but direct evidence at the microscale has been difficult to obtain. Our study reveals the microanatomy and microphysiology of an *Escherichia coli* macrocolony biofilm at an unprecedented cellular resolution, with physiologically different zones and strata forming as a function of known global regulatory networks that respond to biofilm-intrinsic gradients of nutrient supply. In addition, this study identifies zones of heterogeneous and potentially bistable CsgD and curli expression, shows bacterial curli networks to strikingly resemble Alzheimer plaques, and suggests a new role of flagella as an architectural element in biofilms.

Received 8 February 2013 Accepted 13 February 2013 Published 19 March 2013

Citation Serra DO, Richter AM, Klauck G, Mika F, Hengge R. 2013. Microanatomy at cellular resolution and spatial order of physiological differentiation in a bacterial biofilm. *mBio* 4(2):e00103-13. doi:10.1128/mBio.00103-13.

Editor Roberto Kolter, Harvard Medical School

Copyright © 2013 Serra et al. This is an open-access article distributed under the terms of the [Creative Commons Attribution-Noncommercial-ShareAlike 3.0 Unported license](https://creativecommons.org/licenses/by-nc-sa/3.0/), which permits unrestricted noncommercial use, distribution, and reproduction in any medium, provided the original author and source are credited.

Address correspondence to Regine Hengge, Rhengge@zedat.fu-berlin.de.

Bacteria are generally thought of as single-cellular forms of life. However, in their natural environments, they often occur in structured multicellular communities known as biofilms (1–3). Within a biofilm, bacteria are more resistant to antibiotics and disinfectants and can evade the immune system of their hosts (4). As a consequence, chronic infections are often associated with biofilm formation (5). Since bacteria in biofilms can hardly be eradicated, they cause massive damage in medical as well as technical environments (1). The multicellular and sessile biofilm lifestyle is characterized by the expression of adhesins and the production of an extracellular matrix consisting of exopolysaccharides, proteins, and sometimes DNA (6, 7). In contrast, the single-cellular “planktonic” lifestyle is usually associated with the synthesis of flagella and motility. Nevertheless, flagella also seem required to produce a surface-attached biofilm (8, 9), but their actual function within the biofilm has remained uncharacterized.

Experimental investigations of bacterial biofilms have used mainly two model systems: (i) “flow cells,” or microtiter dishes, in

which a submerged biofilm is grown on a chemically inert surface with nutrients provided by the surrounding medium (10, 11), i.e., a setting that mimics an aquatic environment, or (ii) “pellicles” grown on the surface of static liquid medium or “macrocolonies” on agar plates, which—in contrast to the standard colonies of classical microbiology—are grown for extended times, during which they can develop striking morphological patterns (12, 13). The latter resemble biofilms that grow on organic material that provides both support and nutrients.

In this study, we investigate the spatiotemporal development of macrocolony fine structure and physiology using *Escherichia coli* as a model organism. Gram-negative *E. coli* is a physiological generalist (14), a commensal inhabitant of the human intestine as well as a common environmental germ, which also has repeatedly evolved into pathogenic variants that can cause urinary tract infections, hemorrhagic diarrhea, or hemolytic uremic syndrome (15). Like most bacteria, *E. coli* can switch between a planktonic, motile, single-cell state and living in a biofilm (16).

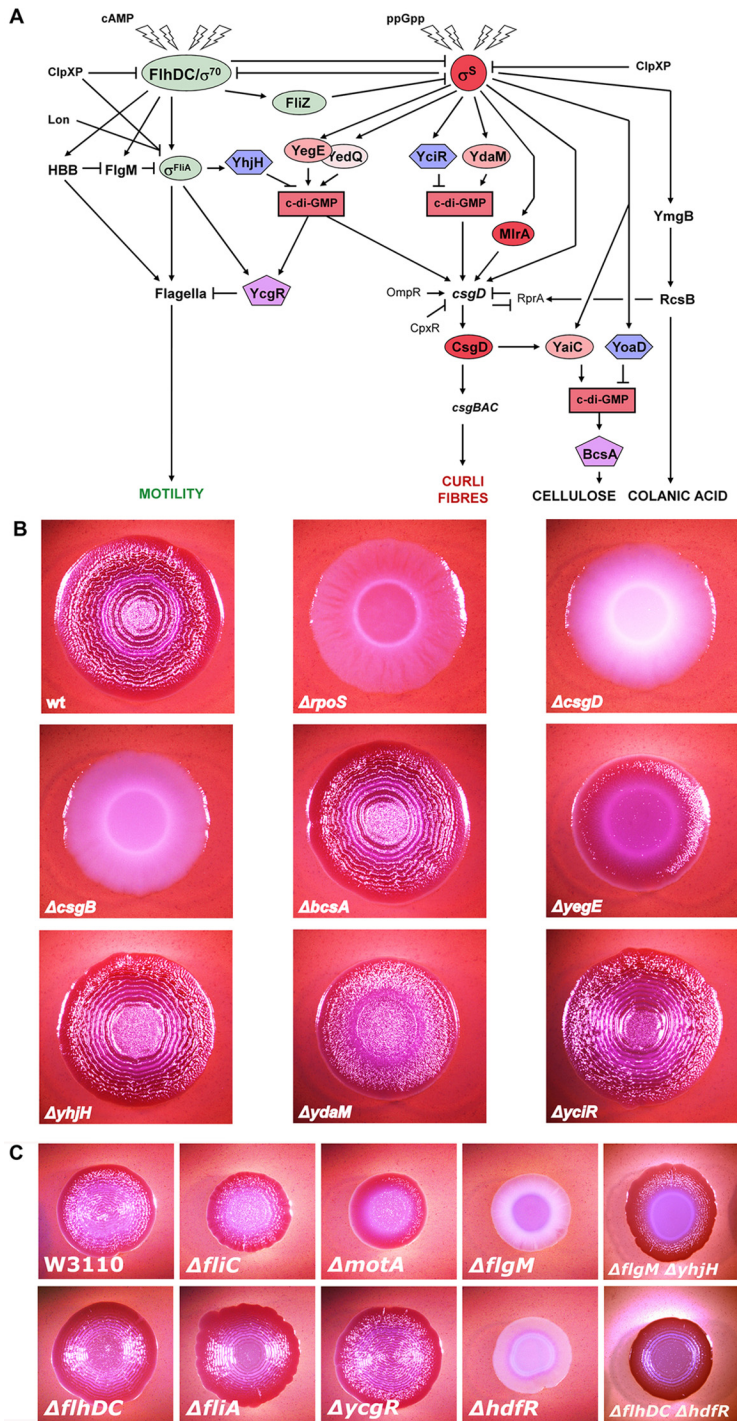


FIG 1 Regulation of flagella, CsgD, and curli and the role of *c*-di-GMP in macrocolony morphology. (A) The regulatory cascade that drives flagellum synthesis and operation (FlhDC/σ⁷⁰, σ^{FlhA}, and its anti-sigma factor, FlgM; left side of the figure) (25) and the transcription factor cascade that drives biosynthesis of curli fibers (σ^S, MirA, CsgD; right side of the figure) inhibit each other by two mechanisms: (i) FlhZ, which is under positive FlhDC control, downregulates a subset of σ^S-dependent genes, including *ydaM*, *mlrA*, and *csgD* (20, 34), and (ii) two separate *c*-di-GMP control modules, each consisting of a diguanylate cyclase(s) (light red ovals) and a phosphodiesterase (blue hexagons), downregulate motility and activate *csgD* transcription (YegE/YedQ and YhjH), or activate *csgD* only (YdaM and YciR) (20, 30). A third *c*-di-GMP control module (YaiC and YoaD) controls the activity of the cellulose synthase BcsA. *c*-di-GMP-binding effectors are shown as purple pentagons. (B and C) Macrocolonies of strain W3110 and the indicated mutant derivatives were grown for 5 days on CR-containing salt-free LB plates.

Being probably the best-understood organism on this planet, *E. coli* provides the opportunity of linking its intricate and well-studied global regulatory networks to the spatiotemporal development of morphological and physiological patterns in biofilms. In more-homogeneous liquid batch cultures, the physiological and genetic characteristics of different lifestyles are associated with different growth phases. In the postexponential growth phase, in which resources are no longer optimal but not yet completely exhausted, *E. coli* cells produce flagella and become highly motile (17–21). Morphologically, cells become successively shorter but are still rod-shaped and continue to divide (22). However, when resources are further on the decline, cells stop producing flagella, they become smaller and ovoid, and they eventually cease to grow and divide and enter into stationary phase—in other words, they give up growth and concentrate on survival (14). In parallel, they begin to produce and excrete autoaggregative curli fibers, a process which leads to cellular aggregation (23). When *E. coli* or related bacteria are grown on agar plates, these curli fibers, which are amyloids and therefore can be stained with Congo red (CR), are essential to generate morphological patterns (12).

These processes are controlled by a complex regulatory circuitry (Fig. 1A) which involves the flagellar master regulator FlhDC and the σ^S (RpoS) subunit of RNA polymerase (RNAP) (14). FlhDC is expressed in the postexponential phase of the growth cycle (21, 24) and controls approximately 60 to 80 genes involved in flagellum synthesis and operation, chemotaxis, and related functions in a three-layer cascade (25, 26). σ^S is the master regulator of the stationary phase and general stress response, which controls the expression of more than 500 genes in a highly complex regulatory network (27, 28). As a consequence, cells with high σ^S activity are in a physiological state quite different from that of growing cells, which is characterized by multiple stress resistances, small ovoid cell morphology, and altered energy metabolism (14). Also, the expression of curli fibers is part of this σ^S-driven stationary phase and general stress response (Fig. 1) (29, 30).

The two master regulators FlhDC and σ^S receive major regulatory input from the two nucleotide second messengers cyclic AMP (cAMP) (31) and guanosine penta/tetraphosphate [(p)ppGpp] (32, 33). The FlhDC-controlled and σ^S-controlled transcriptional cascades—and therefore also the expression of flagella and curli fibers—are inversely coordinated by the DNA-binding protein FlhZ (34) and a third nucleotide messenger, bis-(3′-5′)-cyclic dimeric GMP (*c*-di-GMP) (Fig. 1) (23). *c*-di-GMP is produced and degraded by multiple diguanylate cyclases (DGCs; characterized by GGDEF domains) and phosphodiesterases (PDEs; with EAL domains), respectively. Together with a transcription factor, MirA (35), and σ^S-containing RNAP,

several of these DGCs and PDEs are involved in controlling the expression of CsgD, an essential activator of the curli operon and other biofilm genes (Fig. 1A) (20, 30, 36).

Based on the detailed knowledge of this regulatory network that underlies lifestyle switches in *E. coli*, this study uses cell size and shape, flagella, and curli fibers, as well as visualized expression of the biofilm regulator CsgD, as morphological hallmarks for the different physiological states of cells in various areas of macrocolony biofilms. This allows us to elucidate the spatial order of physiological differentiation in a bacterial biofilm *in situ* at an unprecedented high resolution.

RESULTS

Morphology of the *E. coli* K-12 macrocolony biofilm depends on curli fibers and flagella. When grown on salt-free complex medium below 30°C, where CsgD and curli fibers are expressed (30), macrocolonies of the *E. coli* K-12 strain W3110 developed complex morphology (Fig. 1B; see also Fig. S1 in the supplemental material). The outer region of a macrocolony was characterized by a narrow smooth-growth zone, followed by a zone in which wrinkles began to emerge and then developed into a pattern of somewhat irregular concentric rings. The inner region, which corresponds to the area where the starter bacteria had been applied, eventually also developed into a ring pattern, which, however, took more time (Fig. S1A).

This pattern formation, which was accompanied by intensive staining with the amyloid dye Congo red (CR), was completely abolished in a curli-deficient *csgB* mutant as well as in mutants lacking the regulatory genes *rpoS* and *csgD*, which are essential for curli formation (Fig. 1B). Mutants not containing the DGCs YdaM and YegE, which positively regulate CsgD and, therefore, curli (20, 30), showed only slight wrinkling but did not develop into a ring pattern; eliminating the antagonistic PDE YciR or YhjH seemed to promote the formation of more-pronounced and somewhat more-regular rings (Fig. 1B). Thus, high-level curli production is a prerequisite for the formation of wrinkles and ring-like macrocolony structures. Cellulose is not involved, since *E. coli* K-12 strains are known to not produce cellulose (37, 38) and deletion of the entire cellulose synthase gene *bcsA* in strain W3110 did not alter colony morphology (Fig. 1B).

Since flagella and motility have also been implicated in biofilm formation, we tested whether mutations in the flagellar genetic network affected macrocolony morphology. Mutants that do not produce flagellin (*fliC*) or cannot rotate their flagella (*motA*) were unable to develop a full-fledged ring pattern (Fig. 1C). However, this defect was partially compensated for in mutants defective in the master regulatory gene *flhDC* or the flagellar sigma factor gene *fliA*, which were able to produce ring patterns but hardly any wrinkles before the appearance of the rings (Fig. 1C). Besides not having flagella, these global regulatory mutants have also increased c-di-GMP levels since they do not express the major PDE YhjH (Fig. 1A) (20). This suggested that overproduction of c-di-GMP and curli can generate a ring pattern also in the absence of flagella but that in a wild-type (WT) background, flagella contribute to the initial phase of structure development in which wrinkles begin to appear.

Also, two mutants in the “flagellar series” with unstructured macrocolony morphology point to a major regulatory role for c-di-GMP. These are knockouts in (i) *flgM* (encoding the anti-sigma factor for FliA [25]), which results in higher expression of

all class 3 flagellar genes (including the PDE gene *yhjH*), and (ii) *hdfR* (encoding a repressor of *flhDC*), which leads to higher expression of the entire set of flagellar genes. Ring patterns can be restored by additionally knocking out *yhjH* in the *flgM* mutant as well as by knocking out *flhDC* (and thereby eliminating *yhjH* expression) in the *hdfR* mutant (Fig. 1C). Finally, a deletion of *ycgR*, which encodes a c-di-GMP effector protein that can reduce flagellar rotation speed during stationary phase (20, 39), or of several chemotaxis genes (*cheA*, *cheB*, *cheY*) did not significantly alter macrocolony morphology (Fig. 1C and data not shown).

Overall, we conclude that curli fibers are essential for any structures to develop in *E. coli* K-12 macrocolonies. Flagella make a more subtle contribution, as they are required for initial wrinkling but not for ring formation in the presence of high levels of c-di-GMP. In order to exert this function, flagella have to be able to rotate, but slowing down rotation with increasing c-di-GMP levels or chemotaxis is not required to generate the characteristic long-term macrocolony structure of *E. coli* K-12 W3110.

Curli fibers are restricted to the top and inner biofilm regions and show heterogeneity of expression. In order to determine where in the macrocolony bacteria produce curli fibers, we used a cryosectioning/fluorescence microscopy approach with thioflavin S (TS) as a curli-imaging agent. Thin sectioning allows us to closely examine inner zones of thick structured biofilms which otherwise are difficult to visualize (40, 41). TS shows strong fluorescence upon efficient binding to amyloid fibers and is commonly used in the clinic as an imaging agent for diagnosing amyloid-related disorders (42, 43). The presence of TS in agar plates did not disturb the formation of wrinkle and ring patterns of macrocolonies (see Fig. S1B in the supplemental material).

Low-magnification cross sections through a 7-day-old mature W3110 macrocolony showed a regular series of contiguous dome-like elevations (Fig. 2A) that correspond to the ring pattern observed in the top view of a macrocolony (Fig. 1B). TS fluorescence is highly specific for curli, as it was completely absent in $\Delta csgB$ mutant macrocolonies (Fig. 2B). The spatial distribution and relative intensity of TS fluorescence in these sections showed that curli was highly abundant in the upper layer of the W3110 macrocolony. At higher magnification, TS fluorescence exhibited a “honeycomb” or network-like pattern (Fig. 2C). Further zooming into this fluorescent network showed well-defined silhouettes of bacteria (inset in Fig. 2C), indicating that curli fibers closely surround and interconnect the cells.

Deeper inside the macrocolony, curli expression was observed in distinct patches and often small chains of cells (inset in Fig. 2D), suggesting that once bacteria switch on curli production, this state is maintained in their progeny. Finally, curli expression was completely absent in the lower layer of the macrocolony, i.e., close to the agar interface (Fig. 2A).

Cellular structure and physiological states in different zones of a mature macrocolony biofilm. In order to study the spatial organization and physiological states of bacteria within the macrocolony at the cellular level, we used high-resolution scanning electron microscopy (SEM) and a visual “hallmark” approach based on the detailed knowledge of the regulatory network that controls lifestyle switches and cellular phenotypes in *E. coli* (Fig. 1A). Thus, cell size and shape, the presence or absence of dividing cells, flagella, and curli fibers are used as markers reflecting characteristic physiological states (as detailed in the introduction). Four representative areas of mature macrocolonies were

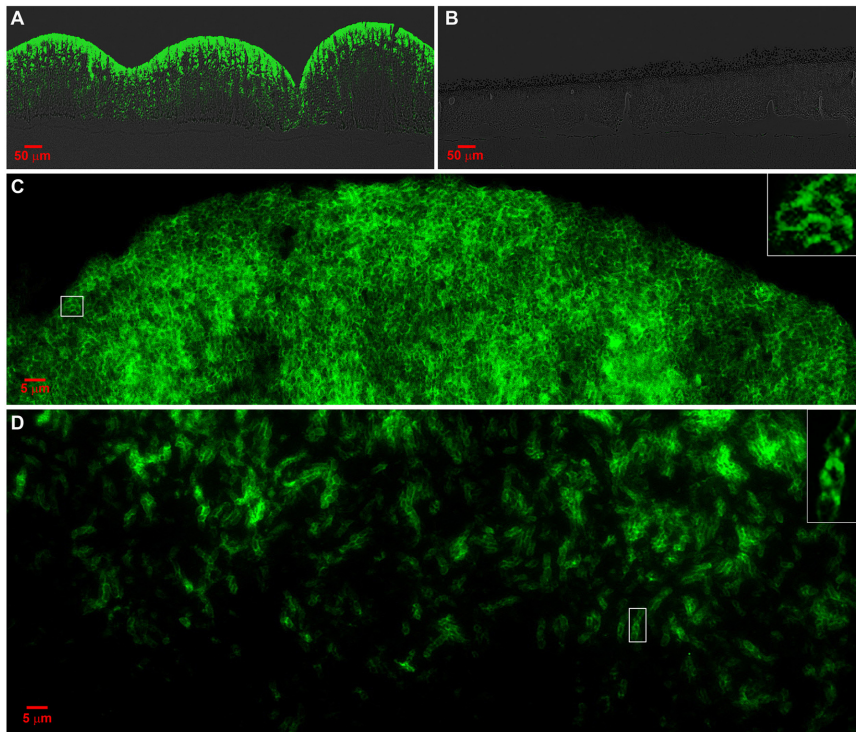


FIG 2 Spatial distribution of curli in different biofilm zones visualized by thioflavin S fluorescence. Seven-day-old *E. coli* macrocolony biofilms grown on salt-free LB medium supplemented with TS were cryoembedded and sectioned perpendicular to the plane of the macrocolony at a thickness of 5 μm . Thin sections were visualized by fluorescence microscopy. Fluorescence images were false-colored green for TS. (A and B) Merged bright-field and fluorescence images at low magnification of representative cross sections of macrocolonies of W3110 and its ΔcsgB derivative, respectively. Images visualize the whole vertical section of the macrocolonies at the central region. Bright-field images appear in a gray background to better visualize the location of the fluorescence. (C and D) Fluorescence images of a representative 5- μm -thick section showing upper and inside-middle parts of the W3110 macrocolony biofilm, respectively. The upper-right insets show enlarged views of the respective boxed areas.

distinguished in this analysis: (i) the outer surface, (ii) the bottom at the agar interface, (iii) the outer colony edge, and (iv) the internal or middle region far away from the other three regions.

(i) Macrocolony surface. Figure 3A shows a perspective view of a fragment of a mature 7-day-old macrocolony of strain W3110 that was mounted upwards on an SEM stub. At larger magnification (Fig. 3B and C), the dome-shaped elevations of the wrinkles/rings were separated by deep crevices. While occasionally showing small fissures and breaks, the surface of the elevated regions appeared rather smooth (Fig. 3C and D), with bacteria being arranged in a plane and almost entirely covered by an extracellular matrix (Fig. 3E and F). Cells were small ($\sim 1 \mu\text{m}$ long) and ovoid, which is a hallmark of severe starvation and stationary phase. In addition, the cells were encased by a dense matrix of filaments. Such features were observed not only at the surface of the wrinkles and rings but in all surface areas of the macrocolony that at the macroscale exhibited CR staining (data not shown). These filaments resembled purified curli fibers as appearing in SEM (44). Moreover, the small and nondividing cells at the surfaces of macrocolonies of the curli-free ΔcsgB and ΔcsgD mutants were “naked,” i.e., devoid of the surrounding filaments (Fig. 3H to I; see also Fig. S2A in the supplemental material), whereas a ΔbcsA mutant was indistinguishable from the parental strain (Fig. S2A). Consequently, this matrix network is composed of curli fibers.

Consistent with TS fluorescence patterns (Fig. 2), the SEM images also showed these curli fibers to assume a “basket”-like structure around the cells. Remarkably, these “custom-molded” baskets (Fig. 3G) did not remain attached to the bacterial cells but maintained their structure even when bacteria were occasionally released from this matrix during the SEM procedure (Fig. S2B).

In toto, based on the small, ovoid anatomy of the cells, their dense encasement by the curli network, and the absence of dividing cells, we conclude that the macrocolony surface is a zone of starvation and stationary-phase physiology. The amyloid curli network confers physical protection to the cells at the surface and, at the same time, promotes cohesion and stability for the macrostructure.

(ii) Macrocolony bottom layer at the agar interface. Our preparation for SEM involves gently floating fixed macrocolonies off the agar blocks, a process which allows us to retrieve macrocolony fragments with bottom-layer regions preserved unaltered that can be examined facing upwards (Fig. 4). This bottom zone consisted of bacterial cells ordered in a plane covered by a dense filamentous mesh. Higher magnification showed the mesh to be formed by long, entangled, and stretched filaments (Fig. 4A and D). While in general this highly dense mesh of filaments nearly obscured the cells, in some areas, it was observed that the fila-

ments originated at the bacterial surface (see Fig. S3 in the supplemental material).

In marked contrast to the macrocolony surface, bacteria in this bottom zone—closer to the nutrient source—were elongated and rod-shaped and also showed evidence of undergoing division. These morphological traits are anatomical hallmarks of *E. coli* in the postexponential growth phase. Knowing that these are also the conditions of flagellum production, we tested whether the filaments observed at the bottom of the macrocolonies were flagella. For this, we analyzed a ΔfliC mutant strain that is unable to produce flagellin and therefore does not assemble flagellar filaments. The mesh of filaments observed for the wild-type strain was completely absent at the bottom of the ΔfliC mutant macrocolony (Fig. 4B and E), with the “naked” bacteria in an organized but fragile spatial arrangement exhibiting the morphological features characteristic of a postexponential-phase physiology. In contrast, the upper surface of the ΔfliC mutant macrocolony looked very similar to that of the parental strain (except for the absence of occasionally occurring single long filaments, suggesting that these were flagella “inherited” from ancestral cells that generations ago had ceased to produce flagella) (see arrows in Fig. S3, upper-right panels, in the supplemental material). Similar results were obtained with an ΔflhDC mutant that does not express any flagellar genes (data not shown). Finally, we found that ΔfimA and ΔdecpRA

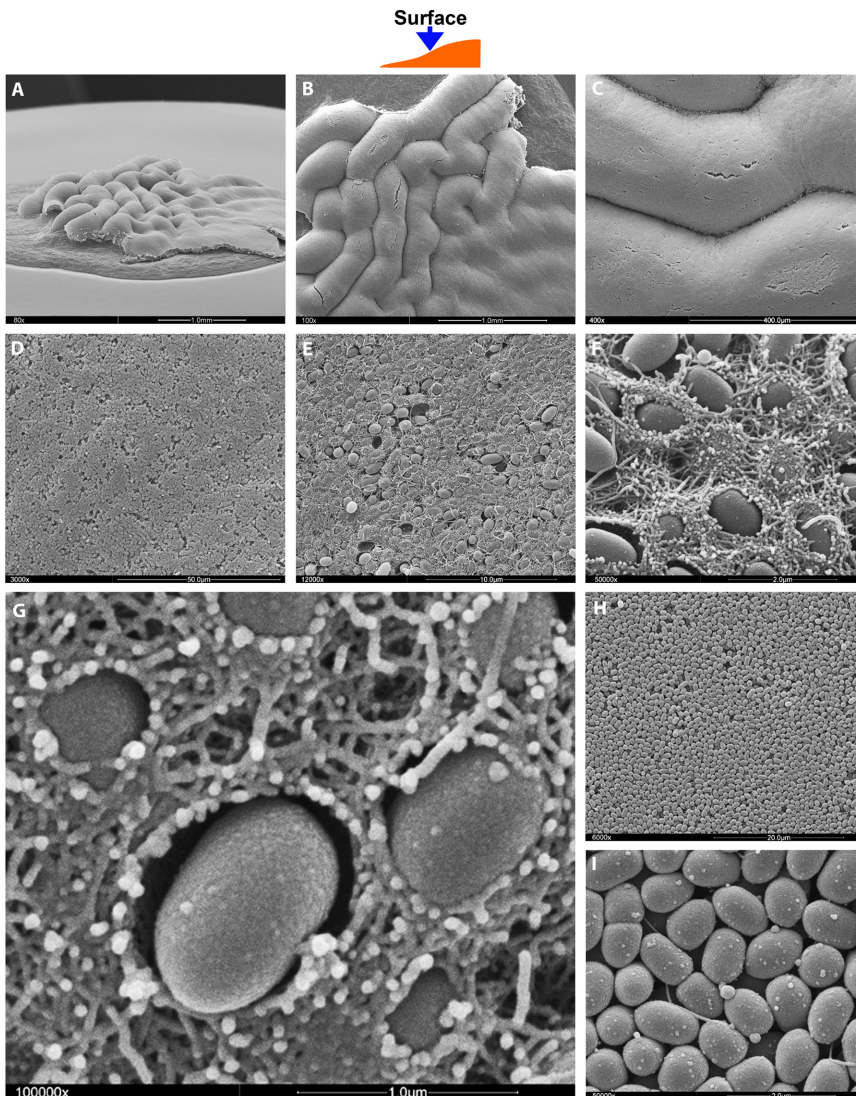


FIG 3 Small, ovoid cells and curli fiber network at the surface of the macrocolony biofilm. Seven-day-old *E. coli* macrocolonies were prepared for SEM examination as described in Materials and Methods. SEM imaging was performed in high vacuum mode. (A) Low-magnification ($\times 80$) perspective-view SEM image of a representative sector of a W3110 macrocolony displaying wrinkles and ring patterns. (B and C) Top-view SEM images at $\times 100$ and $\times 400$ magnification showing the wrinkles of the W3110 macrocolony. (D and E) Further-magnified top views ($\times 3,000$ and $\times 12,000$) of the surface of the wrinkles. (F and G) High-resolution top-view SEM images ($\times 50,000$ and $\times 100,000$) showing in fine detail small, ovoid bacteria encased by a dense network of curli fibers at the surface of a W3110 macrocolony. (H) Top-view SEM image at $\times 6,000$ magnification of the surface of a macrocolony of W3110 $\Delta csgD$. (I) High-resolution top-view SEM image ($\times 50,000$ magnification) showing curli-free, small, ovoid bacteria arranged in a plane at the surface of the $\Delta csgB$ macrocolony.

mutants, which cannot express type 1 fimbriae (45) and *E. coli* common pili (Ecp) (46), respectively, show the same colony morphology and produce the same filamentous mesh at the bottom of the colonies as the parental strain (data not shown). We conclude that this filamentous mesh is composed of flagella.

Rotation of flagella confers motility to planktonic cells. In order to test whether flagellar rotation also contributes to the structure of the flagellar mesh in the bottom zone of the biofilm, we examined a flagellar motor-deficient $\Delta motA$ mutant. In contrast to the stretched appearance of flagella composing the mesh of the

parental strain, flagella of the $\Delta motA$ mutant appeared less entangled but curled up in a more relaxed state (Fig. 4C and F; for even higher resolution, see Fig. S3, lower panels, in the supplemental material). This indicates that flagella become entangled due to their own rotation, i.e., wind around each other and tighten up, which results in many Y-shaped junctions (Fig. S3). Flagellar rotation thereby tethers cells together and contributes to shaping the mesh-like structure at the bottom of the biofilm.

(iii) Macrocolony edges. The outer edge of a mature macrocolony of strain W3110 (Fig. 4G and J) consisted of a very thin and narrow growth zone, which is about $5 \mu\text{m}$ thick (data not shown) and about $20 \mu\text{m}$ wide. This narrow growth zone contained long, rod-shaped cells also tied to each other by entangled flagella (Fig. 4H and I). That flagella play a role in connecting cells was also corroborated by the disintegration of the growth zones of $\Delta fliC$ mutant macrocolonies in almost all of our SEM preparations (data not shown). Only in very few cases was it possible to retrieve intact parts of the growth zone of $\Delta fliC$ mutant macrocolonies that were composed of rod-shaped, nonflagellated cells (Fig. 4K and L).

Adjacent to the narrow outer growth zone, cells became shorter and formed curled patches that at a distance of 40 to $50 \mu\text{m}$ from the edge had developed into a confluent curli layer. Notably, the transition from the growth zone to the confluent curli zone was quite sharp, which allowed us to distinguish areas exclusively inhabited by either relatively long, rod-shaped, flagellated bacteria or ovoid, curli-encased bacteria within a distance of just a few micrometers (Fig. 4J). Overall, the outer rim of a mature macrocolony represents a thin and very narrow zone of postexponential-phase growth, which—during horizontal and vertical expansion of the colony—differentiates into a stationary-phase-like zone at the surface of the macrocolony.

(iv) Stratification of cross-sectioned macrocolonies. The striking morphological difference between the surface and bottom regions as shown above indicated a pronounced stratification of macrocolonies which was corroborated by SEM analysis (see Fig. S4 in the supplemental material). A cross-sectioned mature macrocolony of W3110 has an average height of approximately $260 \mu\text{m}$. Already at low magnification, the surface and upper layers seem more compact than the inner and lower parts of the macrocolony (Fig. S4A). This was due to curli fibers encasing the bacteria and filling up the spaces between the small, ovoid cells

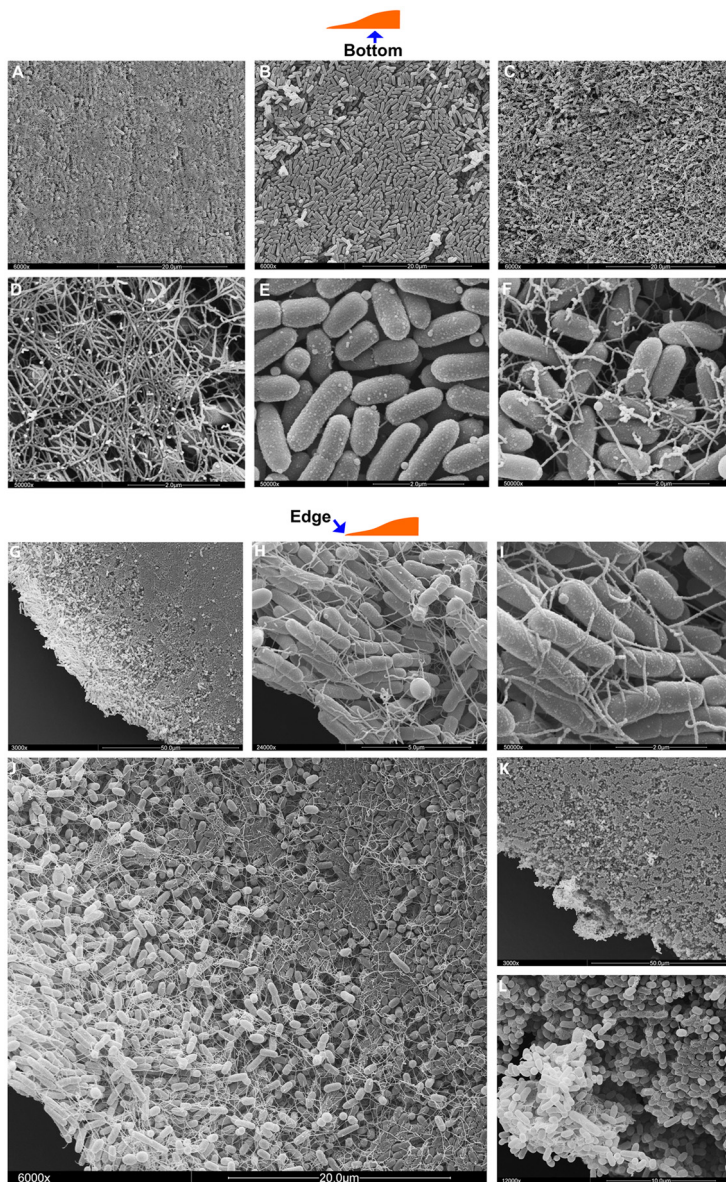


FIG 4 Growing cells and flagella are found at the bottom and the outer rim of the W3110 macrocolony biofilm. (A and D) SEM images at $\times 6,000$ and $\times 50,000$ magnification reveal details of the mesh of entangled filaments formed by bacteria at the bottom of the macrocolony. (B and E) SEM images (also at $\times 6,000$ and $\times 50,000$ magnification) show long, rod-shaped bacteria completely devoid of the filaments at the bottom of a $\Delta fliC$ mutant macrocolony, indicating that the filaments are flagella. (C and F) SEM images of a $\Delta motA$ mutant macrocolony at $\times 6,000$ and $\times 50,000$ magnification show a more relaxed state of the mesh of flagella, which allows coiling of individual flagellar filaments at the bottom of the macrocolony. (G and J) Top-view SEM images (at $\times 3,000$ and $\times 6,000$ magnification) display the outer-edge area of a W3110 macrocolony. (H and I) High-resolution top-view SEM images ($\times 24,000$ and $\times 50,000$) of the outer-edge area show rod-shaped W3110 cells tied together by flagella. (K) The top-view SEM image (at $\times 3,000$ magnification) shows the outer-edge area of a $\Delta fliC$ mutant macrocolony. The image reveals the almost complete loss of the growth zone at the edge, which occurred during the preparation procedure for SEM. (L) Magnified top-view SEM image ($\times 12,000$) of the edge of a $\Delta fliC$ mutant macrocolony. The image shows a remaining sector of the growth zone composed by nonflagellated, rod-shaped cells.

(Fig. S4B and E). Deeper inside the macrocolony, a transition area in which patches and small chains of curli-encased bacteria were found right next to groups of flagellated cells was observed

(Fig. S4C and F). Finally, the lower layers of the macrocolony were inhabited exclusively by longer, flagellated cells that were tied to each other by a net of entangled flagella (Fig. S4D and G). Cross sections through macrocolonies of $\Delta csgB$ and $\Delta fliC$ mutants further substantiated these results. While the $\Delta csgB$ mutant macrocolony was composed of small “naked” bacteria in the upper layers, the $\Delta fliC$ mutant macrocolony featured elongated “naked” bacteria in the bottom layers (Fig. S5).

In summary, these results, along with the TS staining data (Fig. 2), show the physiological stratification inside the macrocolony biofilm: whereas the upper and lower layers are characterized by stationary- and postexponential-phase-like physiologies, respectively, the middle layer represents a transition zone between these two states.

Cellular structure and physiological states in the different zones of a developing macrocolony biofilm. To gain insight into the anatomical and physiological changes during the development of a macrocolony, we also examined “young” macrocolonies grown for 2 days only. We chose this stage because at this time of development, wrinkles begin to form at the surface right next to the outer edges and the first rings begin to appear in the still-thin and mostly flat macrocolony (see Fig. S1A in the supplemental material).

Consistent with the distribution and intensity of CR staining and macromorphological appearance, we distinguished three zones at the young macrocolony surface (Fig. 5A). Zone I, located at the edge of the macrocolony and hardly stained with CR, was a growth zone about 10 times wider than the outer-edge growth zone in 7-day-old macrocolonies. This zone was inhabited by long, rod-shaped, and frequently dividing bacteria that were arranged in parallel to their long axes (Fig. 5B and E). These cells produced flagella that got entangled, thereby tying cells together (Fig. 5B and E, arrows). Zone II was about 1 mm wide and corresponded to the transition zone in which wrinkles started to form. In this zone, bacteria remained organized and tethered together by flagella, but cells were shorter and some started to produce curli fibers, all of which indicates increasing nutrient limitation (Fig. 5C and F). Curli expression was again strikingly heterogeneous, with patches and chains of curli-encased bacteria located right next to curli-free cells at the surface of the colony (Fig. 5C and F, arrows). Zone III encompasses the few rings and the still-flat central part of the macrocolony. At the surface of this zone, each bacterium was already encased in the “custom-molded curli basket” as described above, although the intercellular space seemed less filled up than in mature macrocolonies (Fig. 5D and G).

In order to study the vertical distribution of curli production inside the three zones of the developing macrocolony, we examined cross sections through a 2-day-old macrocolony grown in the presence of TS. Zone I was extremely thin and com-

posed entirely of cells that did not produce curli (Fig. 5H; consistent with the SEM images shown in Fig. 5B and E). In zone II, the macrocolony gained thickness and curli fibers were produced in distinct small patches in the upper layer (Fig. 5I). SEM analysis of the inside of zone II supported these results (Fig. 5L, arrows). Slightly further toward its center, the macrocolony reached a height of approximately 60 μm , which nevertheless allowed us to see the arrangement and shapes of individual cells within the entire vertical extension of the macrocolony (Fig. 5K). Although this young macrocolony is still about 4-fold thinner than a mature macrocolony (compare to Fig. S4A in the supplemental material), its morphological and physiological stratification already resembles that of the latter, i.e., short, ovoid bacteria are encased by a curli network in the upper layers (in zone III) (Fig. 5J and M), short, rod-shaped cells switch on curli production heterogeneously in the transition regions, and the longer, rod-shaped cells at the bottom and the outer edge of the macrocolony do not produce curli.

Expression of the curli regulator CsgD in a developing macrocolony biofilm. In order to further study the heterogeneous onset of curli expression in a developing macrocolony, we analyzed the expression of CsgD, the essential activator of the *csgBAC* curli operon. As shown by Northern blot analysis (Fig. 6A), synthesis of *csgD* mRNA—which produces a characteristic ladder pattern of fragments (47)—was high in 1-day-old macrocolonies and then declined during the following days. Thus, the *csgD* gene is active early during the macrocolony development.

In order to clarify whether *csgD* was heterogeneously expressed within the biofilm, we used cryosectioning/fluorescence microscopy with a 2-day-old macrocolony of strain W3110 carrying a single-copy transcriptional *csgD::gfp* reporter fusion. The upper and upper-middle layers of the central area of macrocolonies (i.e., zone III) of this strain featured big clusters of ovoid bacteria showing intense and relatively homogeneous green fluorescent protein (GFP) fluorescence (Fig. 6B, left panel). The formation of these *csgD::gfp*-expressing cell clusters seemed to start at a relatively sharp transition line in the lower-middle layer of the macrocolony. Here, small isolated patches and little chains of moderately fluorescent cells were observed (Fig. 6B, right panel). These patches develop into early clusters of moderately CsgD^{ON} cells, in which single cells then seem to switch to the higher CsgD expression level characteristic for most of the cells in the mature clusters in the upper layers of the macrocolony.

DISCUSSION

The “visual hallmark” approach allows us to elucidate biofilm architecture and physiology at cellular resolution. In his pioneering work 25 years ago, James Shapiro already reported pattern formation in macrocolonies of *E. coli* and cells of different sizes in different parts of the macrocolonies (48). Today it is widely recognized that biofilms contain different zones that are morphologically and physiologically distinct (10, 11, 49–53). However, direct evidence of physiological differentiation within biofilms at the cellular microscale has been difficult to obtain, and the link to known global regulatory networks has remained obscure.

In this work, we elucidated the spatial order of physiological differentiation in *E. coli* macrocolony biofilms in unprecedented detail by using a “visual cellular hallmark” approach. Technically, our approach is based on high-resolution SEM as well as on fluorescence microscopy after cryosectioning of macrocolonies re-

moved from the agar surface by techniques that preserve their structural integrity. Conceptually, we take advantage of the large and robust body of existing knowledge of the regulatory network that controls global lifestyle switching of *E. coli* (Fig. 1), which includes characteristic morphological changes (for a detailed review, see reference 14).

In short, elongated, rod-shaped cells that divide and produce flagella indicate postexponential-phase physiology, which, at the genetic level, is characterized by highly diverse $\sigma^{70}/\sigma^{\text{FlhA}}$ -driven gene expression modulated by cAMP-cAMP receptor protein (CRP) and Lrp. By this scavenging regime, cells try to optimize growth and proliferation despite limiting resources (19, 21, 54, 55). In contrast, a small, ovoid cell shape, an almost total absence of cell division, and the production of amyloid curli fibers are hallmarks for stationary-phase physiology mainly driven by σ^{S} -dependent gene expression in starving cells (22, 30, 56), with c-di-GMP providing a key trigger (23). By this stationary-phase strategy, which also includes becoming multiple stress resistant (27), cells optimize maintenance and survival. Overall, these different strategies represent the two fundamental and, in fact, opposing states of bacterial life—because of resource limitation in natural environments, bacteria have to make the choice of optimizing either growth or survival. At the molecular level in *E. coli*, this choice is based on the competition of sigma factors for a limiting amount of RNAP core enzyme that is controlled by sensing levels of available nutrients (14, 57, 58).

Within biofilms, nutrient supply is not uniform but, rather, follows gradients (11). Accordingly, *E. coli* cell morphologies were clearly different in each zone of the macrocolonies depending on their relative distance from the nutrient source. At the bottom layers, as well as at the thin outer edges of mature macrocolonies (Fig. 4), i.e., close to the nutrient-providing agar, the morphological appearance of cells indicated postexponential-growth physiology. Further up within the macrocolony biofilm, bacteria can only be starving, which is due, in part, to diffusion limitations but is also because growing bacteria in the lower layers consume most of the nutrients. Consistently, cells in the upper layers exhibit the morphological features characteristic of stationary-phase physiology (Fig. 3). The middle layer inside the macrocolony represents a transition zone of physiological heterogeneity, in which smaller cells that already have switched to the stationary-phase mode and thus have turned on curli fiber production are found side by side with somewhat-more-elongated “naked” cells (Fig. 2; see also Fig. S4 in the supplemental material). Following the same logic, it is also not surprising that in a flow cell-grown biofilm, in which nutrients are supplied by the surrounding liquid medium, growing cells are found in the outer layers whereas severe starvation is experienced by cells inside the “mushroom”-like structures of the biofilm (11, 50).

Interestingly, species-specific differences in metabolic potential can completely reverse this stratification. For *Pseudomonas*, for instance, prolonged exposure to severe anoxia drastically shuts down metabolic activity. Consequently, metabolically inactive cells are found at the bottom of a thick macrocolony biofilm, whereas cells in the aerated upper layers can grow on the nutrients diffusing upwards (40, 59). In contrast, the enteric bacterium *E. coli* is able to grow also under anaerobic conditions at the bottom of a thick macrocolony, therefore showing the opposite physiological stratification of the biofilm such that starving cells populate the top surface.

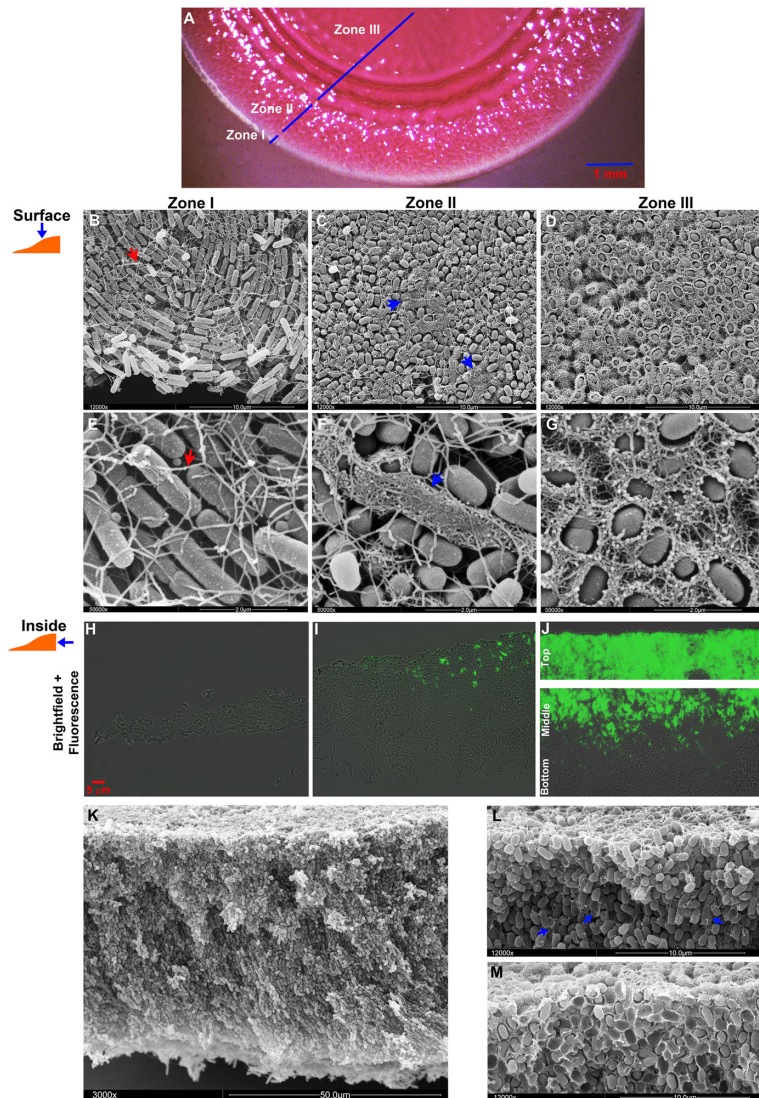


FIG 5 Morphology and horizontal and vertical distributions of flagella and curli in different surface zones of a 2-day-old W3110 macrocolony biofilm. (A) The top-view image shows a 2-day-old macrocolony grown on salt-free LB medium supplemented with CR. (B and E) Top-view SEM images (at $\times 12,000$ and $\times 50,000$ magnification) of the macrocolony surface were taken at zone I as indicated in panel A. Red arrows indicate flagella. (C and F) Top-view SEM images (at $\times 12,000$ and $\times 50,000$ magnification) of the macrocolony surface taken at zone II as indicated in panel A. Blue arrows indicate patches and strips of curli-encased bacteria. (D and G) Top-view SEM images (at $\times 12,000$ and $\times 50,000$ magnification) of the macrocolony surface were taken at zone III as indicated in panel A. (H to J) Merged bright-field and fluorescence images of representative 5- μm -thick cryosections at zones I, II, and III of a 2-day-old W3110 macrocolony grown on salt-free LB supplemented with TS. (K) Side-view SEM image at $\times 3,000$ magnification showing a cross section of a 2-day-old W3110 macrocolony at zone II. (L) Side-view SEM image at $\times 12,000$ magnification of the upper layers of the 2-day-old macrocolony at zone II. Blue arrows indicate curli formation. (M) Side-view SEM images at $\times 12,000$ magnification of the upper layers of the 2-day-old macrocolony at zone III.

Overall, these observations have very general implications. Physiologically, bacterial cells in a multicellular biofilm do not seem fundamentally different from cells in a single-cellular planktonic culture. Rather, the nutrient-dependent temporal succession of the—physiologically highly different—postexponential- and stationary-phase states in a liquid *E. coli* culture translates into

a spatial pattern of physiological differentiation within a biofilm. While for *E. coli* the key determinant seems to be the nutrient gradient, gradients of oxygen, pH, particular stress conditions, signaling molecules, and direct contact of cells with each other or with abiotic or biotic surfaces are also likely to further modulate this physiological differentiation. Despite the extreme complexity of the underlying gene expression control mechanisms, which essentially are stress response control networks (60), it therefore seems that “the biofilm state” is not a specific and distinct developmental state (61). Rather, a biofilm provides a spatially structured form of bacterial life with self-produced gradients and microenvironments (11) which then can allow the onset of specific developmental programs, such as sporulation or competence within the biofilm (41, 49, 62, 63).

Not only for motility—flagella are an architectural element in biofilms. Flagella were produced in the narrow outer edge as well as in the bottom layer of the macrocolony biofilm (Fig. 4), consistent with cells being in the postexponential-growth mode in these regions close to the nutrient-providing agar. This spatial pattern of flagellum expression in macrocolony biofilms may actually be more general. Also, in *Bacillus subtilis*, several flagellar genes (assayed as promoter-*cfp* fusions) were found to be active in the bottom region and the outer rims of macrocolonies, although flagella were not directly visualized (41).

At the interface between *E. coli* cells and the agar surface, flagella formed a strikingly dense mesh. Moreover, flagellar rotation was critical for flagellar filaments to get entangled and tighten up just like “cellular ropes” that tether cells together (Fig. 4). Mutants unable to rotate their flagella or that do not have flagellar filaments at all show reduced macrocolony pattern formation (Fig. 1C), suggesting that the bottom layer of cells tied together by the flagellar mesh provides a stabilizing “baseplate” that supports the wrinkled structure forming in the upper layer during expansion of the macrocolony. In these upper layers of stationary-phase cells, flagella are not produced but still can be found within the curli network, suggesting that existing flagella are not lost but rather become “diluted” by cell proliferation.

Also, at the outer growth edges of the macrocolonies, flagella wrapped around growing cells and tied them together (Fig. 4 and 5). Such a connective function stabilizes the outer colony rim—flagellum-deficient cells had extremely fragile colony edges. It may also contribute to keeping

bacteria ordered during growth, as suggested by images taken of a 2-day-old macrocolony (zone I), in which rod-shaped, flagellum-wrapped bacteria remained in a plane and were arranged in parallel to their long axes (Fig. 5), a multicellular pattern actually already observed by Shapiro (48).

Flagella that tie together bacterial cells in densely packed aggre-

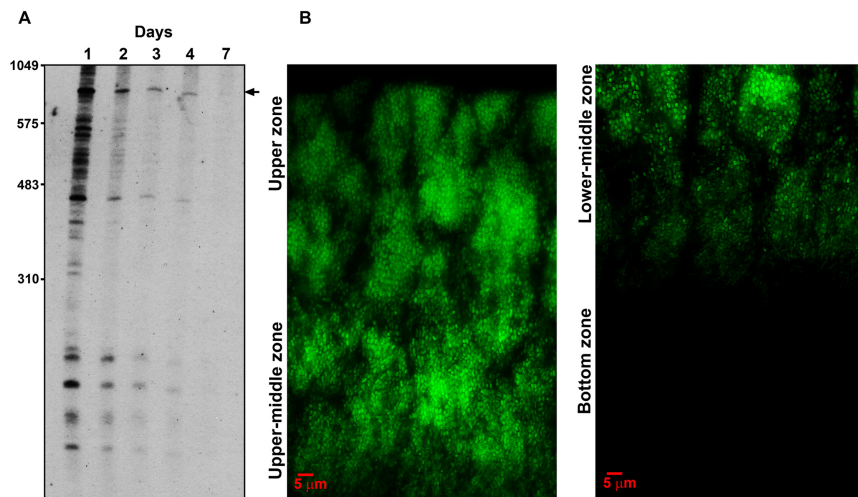


FIG 6 Expression of the key biofilm regulator CsgD in a developing macrocolony biofilm. (A) Cellular levels of *csgD* mRNA in developing W3110 macrocolonies determined by Northern blot analysis. Macrocolonies were harvested after growth for 1, 2, 3, 4, and 7 days as indicated. The arrow indicates the *csgD* mRNA, which is the main product of the *csgDEFG* operon. (B) Expression pattern of *csgD::gfp* in different zones of a representative cross section of a 2-day-old WT macrocolony. Combined, both images visualize the whole vertical section of the macrocolony at the central region (zone III). Macrocolonies of the W3110 derivative harboring a single-copy *csgD::gfp* reporter fusion were grown on salt-free LB plates, cryoembedded, cross-sectioned, and visualized by fluorescence microscopy.

gates are highly unlikely to function as motility-providing organelles. In conclusion, we therefore propose a novel architectural function for flagella within biofilms. Their expression in distinct biofilm regions, together with their ability to tether cells together, may finally explain why flagella are required in many species to form robust biofilms (8, 9, 64, 65).

Curli fiber networks at the biofilm surface are protective and cohesive and resemble Alzheimer plaques. The established link between curli fibers and the stationary-phase physiology (14, 66, 67) already had suggested a protective role of curli fibers. Our images reveal the starving cells of the outer surface layer of an *E. coli* macrocolony to be imbedded in a massive network of curli fibers (Fig. 2 and 3). This network encases cells by custom-molded baskets, which in a mature biofilm do not remain attached to the cell surfaces, although their apparently rigid structure continues to reflect cell shape. Thus, curli fibers do not represent a classical fimbrial adhesin but rather, in a macrocolony biofilm, generate an extracellular macrostructure that confers a compact colony surface, cell-cell cohesion, and protection. In addition, curli fibers contribute to adhesion to abiotic surfaces in other biofilm models (68–72).

Remarkably, this massive curli network in *E. coli* K-12 represents an apparently exclusively proteinaceous biofilm matrix. At the molecular level, curli fibers consist of the nucleator protein CsgB and the major subunit CsgA, which assemble into an amyloid structure in a process tightly controlled by the complex Csg machinery in the cell envelope (44, 73–75). Amyloids are ubiquitous from bacteria to humans and most prominently are associated with human neurodegenerative disorders, such as Alzheimer's disease, in which extracellular amyloid plaques are formed from A β peptide (76). Even at the cellular level, the dense curli network surrounding *E. coli* K-12 cells in our macrocolonies strikingly resembles Alzheimer's A β amyloid plaques (77).

In fact, amyloids are a common structure-stabilizing compo-

nent of the biofilm matrix of many bacterial species (74, 78). A well-studied example is the TasA protein in *Bacillus subtilis* biofilms (13), but uncharacterized amyloids are also abundant in complex natural biofilm communities (79). In general, amyloids coexist with exopolysaccharides in biofilm matrices (3, 6, 13). In “undomesticated” *E. coli* strains, such an exopolysaccharide is cellulose, which in many but not all strains is coregulated with curli (37, 80, 81). However, *E. coli* K-12 does not produce cellulose (37, 38). Also, natural commensal or pathogenic isolates can be cellulose negative (80) and therefore may produce the kind of curli-only matrix that we have observed here for *E. coli* K-12. This may contribute to pathogenicity, since various *E. coli* strains can express curli also at 37°C (80) and curli fibers bind to fibronectin and laminin (67) and are known to be proinflammatory (82, 83).

Heterogeneous and potentially bistable expression of CsgD and curli in the “transition” zones of a macrocolony

biofilm. It was previously shown that macrocolony biofilms of *Salmonella* contain subpopulations of cells with either high or low expression of the curli regulator CsgD, but CsgD expression was not correlated with position within the macrocolony (84). In our study, we observed two regions of transition from flagellum-producing to curli-synthesizing cells: (i) the inner biofilm regions (Fig. 2 and 5) and (ii) the macrocolony surface area close to the edges just adjacent to the smooth-growth zone (Fig. 4 and “zone II” in Fig. 5). In these transition zones, which due to their location probably exhibit similar nutrient limitation, single cells can switch on CsgD and curli production and become surrounded by curli baskets. This curli^{ON} state is then stably maintained in their progeny, which leads to small chains of curliated cells (Fig. 2 and 5). These curliated cells are located immediately adjacent to “naked” cells, i.e., curli expression is clearly heterogeneous within these regions of the biofilm. Many of the “naked” cells, especially the large majority of cells which finally end up in the upper massively curliated layer of the macrocolony, may eventually switch on CsgD and curli expression somewhat later.

Nevertheless, even in the upper areas, large clusters of CsgD-containing cells are interspersed with narrow regions containing cells that have not turned on CsgD synthesis (at a time when average *csgD* mRNA expression in the entire biofilm is already shutting down again) (Fig. 6). This suggests that curli fibers may initially assemble around the producer cells but then also fill up the wider space around these cells, thereby generating the confluent curli network at the surface of the biofilm. Thus, heterogeneity of CsgD and curli expression can occur even in severely starved areas of the biofilm. In addition, vertical streaking of entire clusters of CsgD::GFP-expressing cells (Fig. 6B) and a vertical chain-like orientation of the cells in the growing macrocolony (Fig. 5K) suggest a clonal relationship of cells in the same state, i.e., either curli^{ON} or curli^{OFF}, which may indicate bistability of CsgD and curli expression and epigenetic maintenance of the CsgD/curli

status. Bistability of gene expression, which results in stable bifurcation into distinct subpopulations in a homogeneous microenvironment, can be generated by distinct regulatory motifs, e.g., positive autoregulation and/or mutual inhibition (85). The latter motif is provided by the relationship between *csgD* mRNA and small regulatory RNAs, such as RprA (Fig. 1A) (47), but may also be hidden in the not yet fully understood network of several antagonistically acting diguanylate cyclases and *c*-di-GMP phosphodiesterases that control *csgD* transcription (Fig. 1A) (20, 30).

Conclusion and perspectives. The knowledge about biofilm microanatomy and physiological stratification provided by our study will be a basis for numerous future studies. These will address the specific roles in biofilm formation of all diguanylate cyclases, phosphodiesterases, and other *c*-di-GMP-related proteins in *E. coli* as well as the function of the regulatory network motifs that may generate heterogeneity of CsgD and curli expression. Closer inspection of the development of macrocolonies will reveal how curli properties and its synthesis in distinct regions generate the three-dimensional macrocolony structure, i.e., wrinkles and rings. Another important question is how other matrix components, including cellulose, which is produced by many *E. coli* strains, fit into the biofilm picture at cellular resolution.

MATERIALS AND METHODS

Bacterial strains. All strains used are derivatives of the *E. coli* K-12 strain W3110 (86). The *csgD::cat*, *flgM::cat*, *flhDC::kan*, *fliA::cat*, *fliZ::kan*, *fliC::kan*, *ydaM::cat*, *ycgR::kan*, *yciR::kan*, *yegE::kan*, *yjhH::cat*, and *yjhI::kan* mutations are full open reading frame (ORF) deletion(Δ)/resistance cassette insertions that have been previously described (20, 24, 30). For generating the *csgB::cat*, *bcsA::cat*, *fliC::kan*, *fliK::kan*, *cheA::kan*, *cheB::kan*, *cheY::kan*, *hdfR::cat*, and *motA::kan* mutant derivatives of W3110, the one-step inactivation protocol was applied (87) using oligonucleotide primers listed in Table S1 in the supplemental material. When required, cassettes were flipped out (87). Within the W3110 background, mutations were transferred by P1 transduction (88).

Construction of the single-copy transcriptional *csgD::gfp* reporter fusion. The plasmid pUAB-KD3 for the construction of *gfp* transcriptional fusions is a derivative of pUA66 (89) in which the chloramphenicol resistance cassette (*cat*) flanked by FLP recombination target (FRT) sites and amplified from pKD3 (87) was inserted into the *AvrII* site downstream of *gfp*. This plasmid served as a template in a modified one-step inactivation procedure (87) using oligonucleotides listed in Table S1 in the supplemental material. The PCR-amplified *gfp-cat* cassette was inserted into the fusion point of an existing *csgD::lacZ* translational fusion located at the *att*(λ) site of strain GK1300 {using primers also listed in Table S1, this *csgD*(-756,+549)::*lacZ* reporter fusion had been constructed in plasmid pJL28 as previously described (30); the genotype of GK1300 is W3110 *lacI^q Δ lac(Z-A)::scar* [λ RS45: *csgD*(-756; +549)::*lacZ*(hyb.)]}. After P1 transduction of the newly generated *csgD*(-756; +549)::*gfp* fusion into strain NS429 {W3110 *Δ lac(I-A)::scar* [λ RS45: *csgD*(-756; +549)::*lacZ*(hyb.)] and selection for white colonies, the *cat* cassette was flipped out as described by Datsenko and Wanner (87). The correct flip-out and fusion sequence was confirmed by sequencing of appropriate PCR fragments (GATC Biotech). In addition, maintenance of single lysogeny of the resulting strain (GB1374) was confirmed as specified in Powell et al. (90).

Growth of bacterial macrocolonies. Cells were grown overnight in liquid LB medium (88) under aeration at 37°C. A total of 5 μ l of the overnight cultures was spotted on salt-free LB agar plates. Where indicated, agar plates were supplemented with Congo red (CR; 40 μ g ml⁻¹) and Coomassie brilliant blue (20 μ g ml⁻¹) or thioflavin S (40 μ g ml⁻¹). In order to grow all strains to be compared in parallel on a single agar plate, 140-mm-diameter petri dishes (VWR) were used, allowing the spotting of

up to 25 macrocolonies in a 5-by-5 array on a single plate. Plates with macrocolonies were incubated at 28°C for up to 7 days.

Stereomicroscopy. *E. coli* macrocolony biofilms were visualized at $\times 10$ magnification with a Stemi 2000-C stereomicroscope (Zeiss, Oberkochen, Germany). Digital images were captured with an AxioCam-ICC3 digital camera coupled to the stereomicroscope, operated via the AxioVision 4.8 software (Zeiss).

Cryosectioning of macrocolony biofilms and fluorescence microscopy. Cryosectioning of biofilms was carried out in principle as described previously (41). Briefly, agar blocks containing macrocolony biofilms were cut, placed in disposable cryomold (Tissue-Tek), covered with an embedding agent (Tissue-Tek OCT compound), and fast-frozen in a dry ice/ethanol bath. The cryoembedded macrocolony biofilms were sectioned using an HM560 Cryostat (Thermo Fisher Scientific) set at -20°C. Five-micrometer-thick sections perpendicular to the plane of the macrocolony were obtained using disposable Sec35 blades (Thermo Fisher Scientific). The sections were placed on polylysine-coated microscope slides (Superfrost Plus; Fisher Scientific), fixed in 4% paraformaldehyde in phosphate-buffered saline (PBS) (pH 7.4) for 10 min, and gently rinsed three times with PBS. ProLong 9 Gold antifade reagent (Invitrogen, Carlsbad, CA) was added to the slides as a mounting medium.

Fluorescence detection of bound thioflavin S and green fluorescent protein (GFP) on biofilm sections was performed by using an Axioskop 2 microscope (Zeiss, Oberkochen, Germany) using the following filter configurations: for thioflavin S, excitation = 436 BP/20 nm, emission = 535 BP/30 nm; for GFP, excitation = 470 BP/40 nm (HE), emission = 525 BP/50 nm (HE) (GFP). Samples were visualized at either $\times 100$ or $\times 1,000$ magnification. Digital images were captured with an AxioCam MRm digital camera coupled to the Axioskop 2 microscope using the AxioVision 4.8 software (Zeiss). Where indicated, fluorescence images were superimposed with bright-field images to better show the fluorescence location on the biofilm sections.

Sections of colony biofilms grown in the absence of thioflavin S or containing no GFP fusion were included in each respective experiment as controls in order to determine the background fluorescence for either thioflavin S or GFP.

Scanning electron microscopy of bacterial macrocolonies. Agar blocks containing single macrocolony biofilms were cut out from the plates, placed in glass dishes containing 1% (wt/vol) osmium tetroxide in 0.05 M cacodylate buffer (pH 7.5), and incubated for 45 min at room temperature to allow fixation to proceed. Fixation was followed by four washes with cacodylate buffer. Then macrocolonies were gently floated off the agar blocks, placed in baskets, and subjected to dehydration in a graded alcohol series (30, 50, 70, 90, and 100% ethanol). The dehydrated specimens were dried in a critical point drier (CPD 030; Bal-tec Inc., Balzers, Liechtenstein) with liquid carbon dioxide as a transitional fluid. Throughout the described procedures, the macrocolony biofilms were handled with extreme care in order to maximally preserve their structural integrity. After the drying, macrocolonies or sections of them, representative of different sectors, were mounted on aluminum stubs using double-sided adhesive tape and coated with gold in a sputter coater (SCD-040; Balzers, Union, Liechtenstein). The specimens were examined with an FEI Quanta 200 scanning electron microscope (FEI Co., Hillsboro, OR) operating at an accelerating voltage of 15 kV under high vacuum mode. At least five macrocolonies derived from independent cultures were examined per strain or condition.

RNA extraction and analysis. For RNA purification, macrocolonies were inoculated on salt-free LB plates as described above and were grown at 28°C for 24 h, 48 h, 72 h, 96 h, and 7 days. For RNA preparation and Northern blot analysis, 4 or 1 macrocolony (24 h or all other time points, respectively) was dissolved in Trizol reagent (Invitrogen) to isolate total RNA according to the manufacturer's protocol. Using a probe that binds to the 5' untranslated region (UTR) of *csgD* mRNA, Northern blot analysis was performed as described previously (47).

SUPPLEMENTAL MATERIAL

Supplemental material for this article may be found at <http://mbio.asm.org/lookup/suppl/doi:10.1128/mBio.00103-13/-DCSupplemental>.

Figure S1, JPG file, 2.9 MB.
 Figure S2, JPG file, 2.9 MB.
 Figure S3, JPG file, 2.8 MB.
 Figure S4, JPG file, 2.9 MB.
 Figure S5, JPG file, 2.7 MB.
 Table S1, DOC file, 0.1 MB.

ACKNOWLEDGMENTS

We thank Klaus Hausmann (Institute of Biology—Protozoology, Freie Universität, Berlin) for invaluable technical advice and discussion.

This study was funded by the European Research Council under the European Union's Seventh Framework Programme (ERC-AdG 249780 to R.H.). D.O.S. is the recipient of a postdoctoral fellowship from the Alexander von Humboldt Foundation.

Author contributions: concept and design of study, R.H. and D.O.S.; design of experiments, D.O.S., A.M.R., G.K., F.M., and R.H.; performed experiments, D.O.S., A.M.R., G.K., and F.M.; analysis of data, D.O.S., A.M.R., F.M., and R.H.; writing of the paper, R.H. and D.O.S.

REFERENCES

- Hall-Stoodley L, Costerton JW, Stoodley P. 2004. Bacterial biofilms: from the natural environment to infectious diseases. *Nat. Rev. Microbiol.* 2:95–108.
- Kolter R, Greenberg EP. 2006. Microbial sciences: the superficial life of microbes. *Nature* 441:300–302.
- López D, Vlamakis H, Kolter R. 2010. Biofilms. *Cold Spring Harb. Perspect. Biol.* 2:a000398. <http://dx.doi.org/10.1101/cshperspect.a000398>.
- Anderson GG, O'Toole GA. 2008. Innate and induced resistance mechanisms of bacterial biofilms. *Curr. Top. Microbiol. Immunol.* 322:87–107.
- Burmølle M, Thomsen TR, Fazli M, Dige I, Christensen L, Homøe P, Tvede M, Nyvad B, Tolker-Nielsen T, Givskov M, Moser C, Kirketerp-Møller K, Johansen HK, Høiby N, Jensen PØ, Sørensen SJ, Bjarnsholt T. 2010. Biofilms in chronic infections—a matter of opportunity—monospecies biofilms in multispecies infections. *FEMS Immunol. Med. Microbiol.* 59:324–336.
- Branda SS, Vik S, Friedman L, Kolter R. 2005. Biofilms: the matrix revisited. *Trends Microbiol.* 13:20–26.
- Flemming HC, Wingender J. 2010. The biofilm matrix. *Nat. Rev. Microbiol.* 8:623–633.
- Pratt LA, Kolter R. 1998. Genetic analysis of *Escherichia coli* biofilm formation: roles of flagella, motility, chemotaxis and type I pili. *Mol. Microbiol.* 30:285–293.
- Wood TK, González-Barríos AF, Herzberg M, Lee J. 2006. Motility influences biofilm architecture in *Escherichia coli*. *Appl. Environ. Microbiol.* 72:361–367.
- Harmsen M, Yang L, Pamp SJ, Tolker-Nielsen T. 2010. An update on *Pseudomonas aeruginosa* biofilm formation, tolerance and dispersal. *FEMS Immunol. Med. Microbiol.* 59:253–268.
- Stewart PS, Franklin MJ. 2008. Physiological heterogeneity in biofilms. *Nat. Rev. Microbiol.* 6:199–210.
- Römling U. 2005. Characterization of the rdar morphotype, a multicellular behaviour in Enterobacteriaceae. *Cell. Mol. Life Sci.* 62:1234–1246.
- Romero D, Aguilar C, Losick R, Kolter R. 2010. Amyloid fibers provide structural integrity to *Bacillus subtilis* biofilms. *Proc. Natl. Acad. Sci. U. S. A.* 107:2230–2234.
- Hengge R. 2011. The general stress response in gram-negative bacteria, p 251–289. *In* Storz G, Hengge R (ed), *Bacterial stress responses*. ASM Press, Washington, DC.
- Kaper JB, Nataro JP, Mobley HL. 2004. Pathogenic *Escherichia coli*. *Nat. Rev. Microbiol.* 2:123–140.
- Beloin C, Roux A, Ghigo JM. 2008. *Escherichia coli* biofilms. *Curr. Top. Microbiol. Immunol.* 322:249–289.
- Adler J, Templeton B. 1967. The effect of environmental conditions on the motility of *Escherichia coli*. *J. Gen. Microbiol.* 46:175–184.
- Amsler CD, Cho M, Matsumura P. 1993. Multiple factors underlying the maximum motility of *Escherichia coli* as cultures enter post-exponential growth. *J. Bacteriol.* 175:6238–6244.
- Liu M, Durfee T, Cabrera JE, Zhao K, Jin DJ, Blattner FR. 2005. Global transcriptional programs reveal a carbon source foraging strategy by *Escherichia coli*. *J. Biol. Chem.* 280:15921–15927.
- Pesavento C, Becker G, Sommerfeldt N, Possling A, Tschowri N, Mehli A, Hengge R. 2008. Inverse regulatory coordination of motility and curl-mediated adhesion in *Escherichia coli*. *Genes Dev.* 22:2434–2446.
- Zhao K, Liu M, Burgess RR. 2007. Adaptation in bacterial flagellar and motility systems: from regulon members to “foraging”-like behavior in *E. coli*. *Nucleic Acids Res.* 35:4441–4452.
- Lange R, Hengge-Aronis R. 1991. Growth phase-regulated expression of *bolA* and morphology of stationary-phase *Escherichia coli* cells is controlled by the novel sigma factor σ^S (*rpoS*). *J. Bacteriol.* 173:4474–4481.
- Hengge R. 2010. Role of c-di-GMP in the regulatory networks of *Escherichia coli*, p 230–252. *In* Wolfe AJ, Visick KL (ed), *The second messenger cyclic-di-GMP*. ASM Press, Washington, DC.
- Barembuch C, Hengge R. 2007. Cellular levels and activity of the flagellar sigma factor FliA of *Escherichia coli* are controlled by FlgM-modulated proteolysis. *Mol. Microbiol.* 65:76–89.
- Chevance FF, Hughes KT. 2008. Coordinating assembly of a bacterial macromolecular machine. *Nat. Rev. Microbiol.* 6:455–465.
- Girgis HS, Liu Y, Ryu WS, Tavazoie S. 2007. A comprehensive genetic characterization of bacterial motility. *PLoS Genet.* 3:e154. <http://dx.doi.org/10.1371/journal.pgen.0030154>.
- Lange R, Hengge-Aronis R. 1991. Identification of a central regulator of stationary-phase gene expression in *Escherichia coli*. *Mol. Microbiol.* 5:49–59.
- Weber H, Polen T, Heuveling J, Wendisch VF, Hengge R. 2005. Genome-wide analysis of the general stress response network in *Escherichia coli*: σ^S dependent genes, promoters, and sigma factor selectivity. *J. Bacteriol.* 187:1591–1603.
- Römling U, Bian Z, Hammar M, Sierralta WD, Normark S. 1998. Curli fibers are highly conserved between *Salmonella typhimurium* and *Escherichia coli* with respect to operon structure and regulation. *J. Bacteriol.* 180:722–731.
- Weber H, Pesavento C, Possling A, Tischendorf G, Hengge R. 2006. Cyclic-di-GMP-mediated signalling within the sigma network of *Escherichia coli*. *Mol. Microbiol.* 62:1014–1034.
- Botsford JL, Harman JG. 1992. Cyclic AMP in prokaryotes. *Microbiol. Rev.* 56:100–122.
- Magnusson LU, Farewell A, Nyström T. 2005. ppGpp: a global regulator in *Escherichia coli*. *Trends Microbiol.* 13:236–242.
- Potrykus K, Cashel M. 2008. (p)ppGpp: still magical? *Annu. Rev. Microbiol.* 62:35–51.
- Pesavento C, Hengge R. 2012. The global repressor FliZ antagonizes gene expression by σ^S containing RNA polymerase due to overlapping DNA binding specificity. *Nucleic Acids Res.* 40:4783–4793.
- Brown PK, Dozois CM, Nickerson CA, Zuppardo A, Terlonge J, Curtiss R, III. 2001. MlrA, a novel regulator of curli (Agf) and extracellular matrix synthesis by *Escherichia coli* and *Salmonella enterica* serovar typhimurium. *Mol. Microbiol.* 41:349–363.
- Sommerfeldt N, Possling A, Becker G, Pesavento C, Tschowri N, Hengge R. 2009. Gene expression patterns and differential input into curli fimbriae regulation of all GGDEF/EAL domain proteins in *Escherichia coli*. *Microbiology* 155:1318–1331.
- Da Re S, Ghigo JM. 2006. A CsgD-independent pathway for cellulose production and biofilm formation in *Escherichia coli*. *J. Bacteriol.* 188:3073–3087.
- Zogaj X, Nitz M, Rohde M, Bokranz W, Römling U. 2001. The multicellular morphotypes of *Salmonella typhimurium* and *Escherichia coli* produce cellulose as the second component of the extracellular matrix. *Mol. Microbiol.* 39:1452–1463.
- Boehm A, Kaiser M, Li H, Spangler C, Kasper CA, Ackermann M, Kaever V, Sourjik V, Roth V, Jenal U. 2010. Second messenger-mediated adjustment of bacterial swimming velocity. *Cell* 141:107–116.
- Lenz AP, Williamson KS, Pitts B, Stewart PS, Franklin MJ. 2008. Localized gene expression in *Pseudomonas aeruginosa* biofilms. *Appl. Environ. Microbiol.* 74:4463–4471.
- Vlamakis H, Aguilar C, Losick R, Kolter R. 2008. Control of cell fate by the formation of an architecturally complex bacterial community. *Genes Dev.* 22:945–953.
- Fowler DM, Koulov AV, Alory-Jost C, Marks MS, Balch WE, Kelly JW. 2006. Functional amyloid formation within mammalian tissue. *PLoS Biol.* 4:e6. <http://dx.doi.org/10.1371/journal.pbio.0040006>.

43. Westermarck GT, Johnson KH, Westermarck P. 1999. Staining methods for identification of amyloid in tissue. *Methods Enzymol.* 309:3–25.
44. Chapman MR, Robinson LS, Pinkner JS, Roth R, Heuser J, Hammar M, Normark S, Hultgren SJ. 2002. Role of *Escherichia coli* curli operons in directing amyloid fiber formation. *Science* 295:851–855.
45. Sauer FG, Mulvey MA, Schilling JD, Martinez JJ, Hultgren SJ. 2000. Bacterial pili: molecular mechanisms of pathogenesis. *Curr. Opin. Microbiol.* 3:65–72.
46. Blackburn D, Husband A, Saldana Z, Nada RA, Klena J, Qadri F, Girón JA. 2009. Distribution of the *Escherichia coli* common pilus among diverse strains of human enterotoxigenic *E. coli*. *J. Clin. Microbiol.* 47:1781–1784.
47. Mika F, Busse S, Possling A, Berkholz J, Tschowri N, Sommerfeldt N, Pruteanu M, Hengge R. 2012. Targeting of *csfD* by the small regulatory RNA RprA links stationary phase, biofilm formation and cell envelope stress in *Escherichia coli*. *Mol. Microbiol.* 84:51–65.
48. Shapiro JA. 1987. Organization of developing *Escherichia coli* colonies viewed by scanning electron microscopy. *J. Bacteriol.* 169:142–156.
49. Aguilar C, Vlamakis H, Losick R, Kolter R. 2007. Thinking about *Bacillus subtilis* as a multicellular organism. *Curr. Opin. Microbiol.* 10: 638–643.
50. An D, Parsek MR. 2007. The promise and peril of transcriptional profiling in biofilm communities. *Curr. Opin. Microbiol.* 10:292–296.
51. Parsek MR, Greenberg EP. 2005. Sociomicrobiology: the connections between quorum sensing and biofilms. *Trends Microbiol.* 13:27–33.
52. Rani SA, Pitts B, Beyenal H, Veluchamy RA, Lewandowski Z, Davison WM, Buckingham-Meyer K, Stewart PS. 2007. Spatial patterns of DNA replication, protein synthesis, and oxygen concentration within bacterial biofilms reveal diverse physiological states. *J. Bacteriol.* 189:4223–4233.
53. Wimpenny J, Manz W, Szewzyk U. 2000. Heterogeneity in biofilms. *FEMS Microbiol. Rev.* 24:661–667.
54. Ferenci T. 2001. Hungry bacteria—definition and properties of a nutritional state. *Environ. Microbiol.* 3:605–611.
55. Traxler MF, Zacharia VM, Marquardt S, Summers SM, Nguyen HT, Stark SE, Conway T. 2011. Discretely calibrated regulatory loops controlled by ppGpp partition gene induction across the ‘feast to famine’ gradient in *Escherichia coli*. *Mol. Microbiol.* 79:830–845.
56. Santos JM, Freire P, Vicente M, Arraiano CM. 1999. The stationary-phase morphogene *bolA* from *Escherichia coli* is induced by stress during early stages of growth. *Mol. Microbiol.* 32:789–798.
57. Ferenci T. 2005. Maintaining a healthy SPANC balance through regulatory and mutational adaptation. *Mol. Microbiol.* 57:1–8.
58. Nyström T. 2004. Growth versus maintenance: a trade-off dictated by RNA polymerase availability and sigma factor competition? *Mol. Microbiol.* 54:855–862.
59. Williamson KS, Richards LA, Perez-Osorio AC, Pitts B, McInerney K, Stewart PS, Franklin MJ. 2012. Heterogeneity in *Pseudomonas aeruginosa* biofilms includes expression of ribosome hibernation factors in the antibiotic-tolerant subpopulation and hypoxia-induced stress response in the metabolically active population. *J. Bacteriol.* 194:2062–2073.
60. Storz G, Hengge R (ed). 2011. Bacterial stress responses. ASM Press, Washington, DC.
61. O’Toole G, Kaplan HB, Kolter R. 2000. Biofilm formation as microbial development. *Annu. Rev. Microbiol.* 54:49–79.
62. Branda SS, González-Pastor JE, Ben-Yehuda S, Losick R, Kolter R. 2001. Fruiting body formation by *Bacillus subtilis*. *Proc. Natl. Acad. Sci. U. S. A.* 98:11621–11626.
63. Lopez D, Vlamakis H, Kolter R. 2009. Generation of multiple cell types in *Bacillus subtilis*. *FEMS Microbiol. Rev.* 33:152–163.
64. O’Toole GA, Kolter R. 1998. Initiation of biofilm formation in *Pseudomonas fluorescens* WCS365 proceeds via multiple, convergent signalling pathways: a genetic analysis. *Mol. Microbiol.* 28:449–461.
65. Watnick PI, Lauriano CM, Klose KE, Croal L, Kolter R. 2001. The absence of a flagellum leads to altered colony morphology, biofilm development and virulence in *Vibrio cholerae* O139. *Mol. Microbiol.* 39: 223–235.
66. Hammar M, Arnqvist A, Bian Z, Olsén A, Normark S. 1995. Expression of two *csf* operons is required for production of fibronectin- and Congo red-binding curli polymers in *Escherichia coli* K-12. *Mol. Microbiol.* 18: 661–670.
67. Olsén A, Jonsson A, Normark S. 1989. Fibronectin binding mediated by a novel class of surface organelles on *Escherichia coli*. *Nature* 338:652–655.
68. Austin JW, Sanders G, Kay WW, Collinson SK. 1998. Thin aggregative fimbriae enhance *Salmonella enteritidis* biofilm formation. *FEMS Microbiol. Lett.* 162:295–301.
69. Beloin C, Houry A, Froment M, Ghigo JM, Henry N. 2008. A short-time scale colloidal system reveals early bacterial adhesion dynamics. *PLoS Biol.* 6:e167. <http://dx.doi.org/10.1371/journal.pbio.0060167>.
70. Cookson AL, Cooley WA, Woodward MJ. 2002. The role of type 1 and curli fimbriae of Shiga toxin-producing *Escherichia coli* in adherence to abiotic surfaces. *Int. J. Med. Microbiol.* 292:195–205.
71. May T, Okabe S. 2008. *Escherichia coli* harboring a natural IncF conjugative F plasmid develops complex mature biofilms by stimulating synthesis of colanic acid and curli. *J. Bacteriol.* 190:7479–7490.
72. Vidal O, Longin R, Prigent-Combaret C, Dorel C, Hooreman M, Lejeune P. 1998. Isolation of an *Escherichia coli* K-12 mutant strainable to form biofilms on inert surfaces: involvement of a new *ompR* allele that increases curli expression. *J. Bacteriol.* 180:2442–2449.
73. Barnhart MM, Chapman MR. 2006. Curli biogenesis and function. *Annu. Rev. Microbiol.* 60:131–147.
74. Blanco LP, Evans ML, Smith DR, Badtke MP, Chapman MR. 2012. Diversity, biogenesis and function of microbial amyloids. *Trends Microbiol.* 20:66–73.
75. Dueholm MS, Nielsen SB, Hein KL, Nissen P, Chapman M, Christiansen G, Nielsen PH, Otzen DE. 2011. Fibrillation of the major curli subunit CsgA under a wide range of conditions implies a robust design of aggregation. *Biochemistry* 50:8281–8290.
76. Harrison RS, Sharpe PC, Singh Y, Fairlie DP. 2007. Amyloid peptides and proteins in review. *Rev. Physiol. Biochem. Pharmacol.* 159:1–77.
77. Friedrich RP, Tepper K, Rönicker R, Soom M, Westermann M, Reymann K, Kaether C, Fändrich M. 2010. Mechanism of amyloid plaque formation suggests an intracellular basis of A β pathogenicity. *Proc. Natl. Acad. Sci. U. S. A.* 107:1942–1947.
78. Sawyer EB, Claessen D, Gras SL, Perrett S. 2012. Exploiting amyloid: how and why bacteria use cross- β fibrils. *Biochem. Soc. Trans.* 40: 728–734.
79. Larsen P, Nielsen JL, Dueholm MS, Wetzel R, Otzen D, Nielsen PH. 2007. Amyloid adhesins are abundant in natural biofilms. *Environ. Microbiol.* 9:3077–3090.
80. Bokranz W, Wang X, Tschäpe H, Römling U. 2005. Expression of cellulose and curli fimbriae by *Escherichia coli* isolated from the gastrointestinal tract. *J. Med. Microbiol.* 54:1171–1182.
81. Monteiro C, Saxena I, Wang X, Kader A, Bokranz W, Simm R, Nobles D, Chromek M, Brauner A, Brown RM, Jr, Römling U. 2009. Characterization of cellulose production in *Escherichia coli* Nissle 1917 and its biological consequences. *Environ. Microbiol.* 11:1105–1116.
82. Tükel C, Wilson RP, Nishimori JH, Peshki M, Chromy BA, Bäumlér AJ. 2009. Responses to amyloids of microbial and host origin are mediated through Toll-like receptor 2. *Cell Host Microbe* 6:45–53.
83. Tükel C, Nishimori JH, Wilson RP, Winter MG, Keestra AM, van Putten JP, Bäumlér AJ. 2010. Toll-like receptors 1 and 2 cooperatively mediate immune responses to curli, a common amyloid from enterobacterial biofilms. *Cell. Microbiol.* 12:1495–1505.
84. Grantcharova N, Peters V, Monteiro C, Zakikhany K, Römling U. 2010. Bistable expression of CsgD in biofilm development of *Salmonella enterica* serovar Typhimurium. *J. Bacteriol.* 192:456–466.
85. Dubnau D, Losick R. 2006. Bistability in bacteria. *Mol. Microbiol.* 61: 564–572.
86. Hayashi K, Morooka N, Yamamoto Y, Fujita K, Isono K, Choi S, Ohtsubo E, Baba T, Wanner BL, Mori H, Horiuchi T. 2006. Highly accurate genome sequences of *Escherichia coli* K-12 strains MG1655 and W3110. *Mol. Syst. Biol.* 2:2006.0007. <http://dx.doi.org/10.1038/msb4100049>.
87. Datsenko KA, Wanner BL. 2000. One-step inactivation of chromosomal genes in *Escherichia coli* K-12 using PCR products. *Proc. Natl. Acad. Sci. U. S. A.* 97:6640–6645.
88. Miller JH. 1972. Experiments in molecular genetics. Cold Spring Harbor Laboratory, Cold Spring Harbor, NY.
89. Zaslavsky A, Mayo AE, Rosenberg R, Bashkin P, Sberro H, Tsalyuk M, Surette MG, Alon U. 2004. Just-in-time transcription program in metabolic pathways. *Nat. Genet.* 36:486–491.
90. Powell BS, Court DL, Nakamura Y, Rivas MP, Turnbough CL, Jr. 1994. Rapid confirmation of single copy lambda prophage integration by PCR. *Nucleic Acids Res.* 22:5765–5766.